JOURNAL OF MATERIALS SCIENCE 33 (1998) 3109–3119

Alumina–alloy nanocomposite powders by mechanosynthesis

D. OSSO, O. TILLEMENT, G. LE CAER, A. MOCELLIN
LSG2M, UMR CNRS 7584, Ecole des Mines, F-54042 Nancy Cedex France
E-mail: lecaen@mines.u-nancy.fr

Mössbauer spectroscopy and X-ray diffraction were used to investigate the synthesis of nanocomposite powders by reactive milling of a variety of blends of aluminium and metallic oxides corresponding to the target compositions: Al_2O_3–(Fe,Cr,Ni) alloys. Particular emphasis was given to the (Fe,Cr) and (Fe,Ni) binaries with chromium contents ranging between 0.13 and 0.60 and nickel contents between 0.10 and 0.80, respectively. Several compositions in the iron-rich part of the ternary with chromium in the 0.18–0.20 range were also investigated. The essential steps of the reaction mechanisms were identified as functions of milling time and initial composition. A number of transient phases, some metastable under normal conditions at room temperature were observed. Chemical heterogeneities and their changes in the metallic phases were also characterized semi-quantitatively and the possibility of side effects, such as partial dissolution of not yet reacted Cr_2O_3 into newly formed Al_2O_3, was considered. Finally, some of the as-milled powders were subsequently heat treated for 1 h at 1100 °C to explore their structural changes and progress towards homogenization via the same experimental techniques.

1. Introduction

The toughening of brittle ceramics by ductile metals is of considerable interest and much attention has already been devoted to the aim of combining these materials in order to generate new materials with improved properties [1–5]. Within this frame, several processes have been investigated in order to synthesize alumina–metal composites [6–10]. In spite of that, such materials suffer from poor thermal shock resistance and metal–ceramic interfacial weak cohesion. The use of nanostructured cermets could be a way to improve the mechanical properties of such alumina–metal composites.

Mechanochemical reactions induced by milling or grinding of powder mixtures of ceramics and metals may constitute promising processes for the production of nanocermets [11–13]. The possibility of performing displacement reactions by ball milling instead of heating [14] has been used to synthesize various metal–ceramic composite powders [11, 15–22]. According to the composition and milling conditions, an incubation time from 5–150 min for the start of the reduction reaction is generally reported [21] and a large heat of reaction is released. Such reactions may exhibit unstable combustion or progressive behaviour depending on the experimental conditions and the thermodynamics of the metal–metal oxide system [23, 24].

Future applications would probably require extra degrees of freedom such as those provided by alloying various metallic phases in alumina but few studies have concerned such composites synthesized by reactive milling [14, 25]. Only papers devoted to metallic (Fe,Cr) and (Fe,Ni) alloys synthesized by grinding are found in the literature [26–28].

In the present paper, we describe the synthesis of alumina–alloys (Fe,Cr,Ni) composite powders by reduction of a mixture of metal oxides by aluminium powders during ball milling. The exchange reactions of binary (Fe,Cr) and (Fe,Ni)–alumina and ternary (Fe,Cr,Ni)–alumina systems were investigated. Greater attention has been paid to the study of the reaction mechanisms of the two binary systems and to the effects of heat treatments on the evolution of the as-milled powders, as it will generally be attempted to consolidate them into solid sintered pieces.

2. Experimental procedure

Reduction experiments were performed in a planetary ball mill (Fritsch Pulverisette 5) with hardened steel (Z30C13 alloy) vial and balls under an argon atmosphere. A powder to ball weight ratio of 1/20 and a rotation speed of 350 r.p.m. were used for all the experiments. Milling was performed for 8 h with the exception of the mechanism studies, where the time was varied from 10 min to 8 h. The starting commercial powders were aluminium (99.5% pure with average particle size of 1.5 μm) and metal oxides (chromia (Cr_2O_3), haematite (Fe_2O_3) and nickel oxide (NiO), all 99% pure with average particle sizes ranging between 0.5 and 1 μm). The powder mixtures were milled in the

stoichiometric proportions of the expected reaction

$$\frac{(3-y)}{3}\mathrm{Al} + \frac{(1-x-y)}{2}\mathrm{Fe_2O_3} + \frac{x}{2}\mathrm{Cr_2O_3} + y\mathrm{NiO}$$

$$\rightarrow \frac{(3-y)}{6}\mathrm{Al_2O_3} + (1-x-y)\,\mathrm{Fe} + x\mathrm{Cr} + y\mathrm{Ni} \quad (1)$$

The investigated systems will be referred to as Al_2O_3–$Fe_{(1-x-y)}Cr_xNi_y$ as expected from the composition of the initial powder mixture of aluminium and metal oxides.

The as-milled products were characterized by X-ray diffraction (XRD) using CoK_α radiation ($\lambda = 0.178\,89$ nm) and by ^{57}Fe Mössbauer spectroscopy. ^{57}Fe Mössbauer spectra were obtained at room temperature (RT) in transmission geometry with a spectrometer operated in the conventional constant acceleration mode. A ^{57}Co source in rhodium with a strength of ~ 20 mCi was used. The magnetic components of spectra were analysed as distributions of hyperfine magnetic fields $P(H)$ by a conventional constrained Hesse–Rübatsch method [29, 30]. Lorentzian lineshapes were employed in this procedure. The hyperfine parameters of the central paramagnetic components were calculated separately with a least-squares fitting program and were kept constant in the final HMFD fitting step. As usual, the ^{57}Fe isomer shifts are given with respect to α-Fe at RT. The mean crystallite size, $\langle d \rangle$, was calculated using the full-width at half-maximum of X-ray diffraction peaks corrected by the instrumental broadening as described elsewhere [14]. Heat treatments were performed for 60 min at various temperatures up to 1100 °C under an argon flux. Samples were brought to the desired temperature at a heating rate of 10 K min^{-1}. The temperature of 1100 °C corresponds to the upper temperature at which grains constituting the as-milled powder particles still remain in the nanometre range ($t < 100$ nm) in spite of incipient grain growth [31].

3. Results

Reaction 1 was more particularly investigated for the following composition ranges: ($0.13 < x < 0.70$), ($0.10 < y < 1$) and $(x, y) = ([0.20;0.08], [0.20;0.16], [0.20;0.22], [0.18;0.22])$. Three different reaction behaviours were observed in our experimental conditions. For chromium-based systems ($x > 0.6$), the reduction reaction was very slow (progressive reaction). Even after milling for 8 h, the chromium oxide was not totally reduced. In contrast, haematite was fully reduced. Finally, highly exothermic reactions took place in nickel-based systems ($y > 0.80$) and displayed explosive characteristics. Between those two extreme cases, a wide range of mixed oxide compositions exhibit a combustive reaction which consists of a fast oxide reduction because no metal oxide was detected after milling for 8 h. Only the experimental results characterizing the combustive reaction systems will be discussed below.

The composition of the starting mixture did not influence the final average sizes of the crystallites of either ceramic or metallic phases. Almost constant values of 15–20 nm were calculated for the latter in all the investigated alumina–alloy powders.

3.1. Alumina–(Fe,Cr) systems

The mechanism of the reduction reaction for aluminium–(Fe,Cr) oxide systems was studied for the expected Al_2O_3–$Fe_{0.87}Cr_{0.13}$ composition of the as-milled composite. The choice of a composition of 13 at % chromium was made to minimize the effects of contamination by the steel which constitutes the grinding tools whose composition is close to $Fe_{0.87}Cr_{0.13}$.

The displacement reaction started after 10 min milling. Total reduction of iron was achieved after milling for 30 min as revealed by Mössbauer spectroscopy (Fig. 1) and no more chromia was detected by XRD (Fig. 2). In the sample ground for 15 min, i.e. during

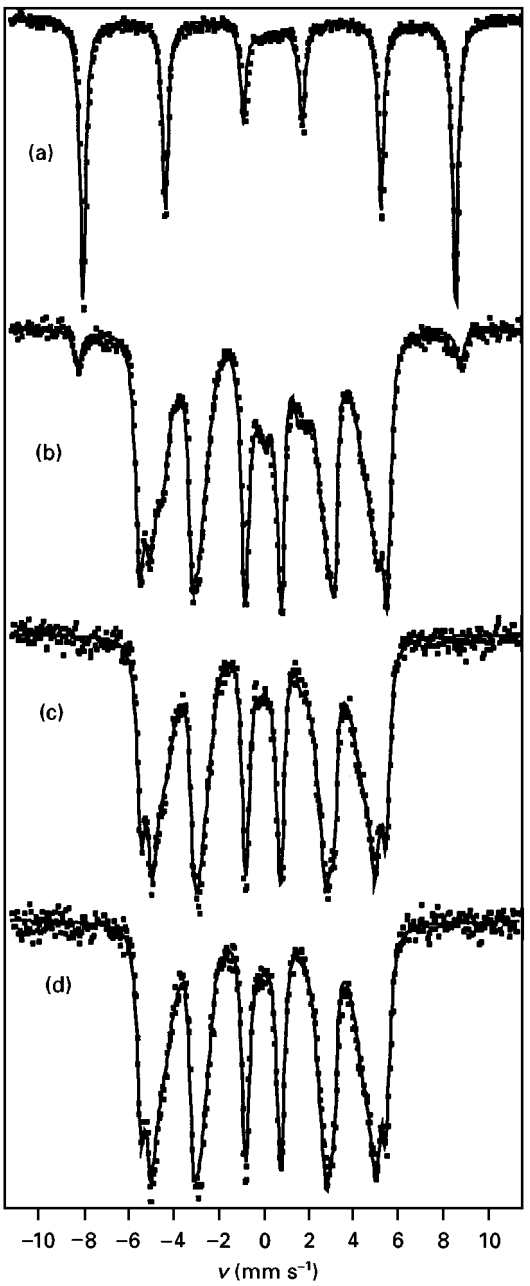

Figure 1 ^{57}Fe room-temperature Mössbauer spectra of $Fe_{0.87}Cr_{0.13}$–Al_2O_3 powders as a function of milling time (a) 10 min, (b) 15 min, (c) 30 min, (d) 120 min.

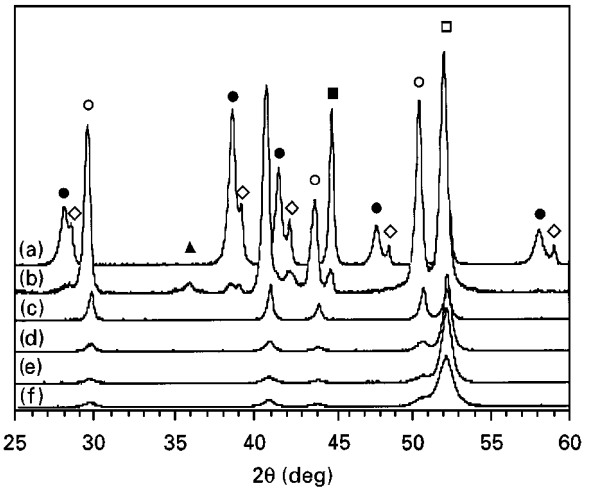

Figure 2 XRD patterns of $Fe_{0.87}Cr_{0.13}$–Al_2O_3 powders as a function of milling time: (a) 13 min, (b) 15 min, (c) 30 min, (d) 60 min, (e) 120 min, (f) 240 min. (▲) $FeAl_2O_4$, (□) Fe, (○) α-Al_2O_3, (●) Fe_2O_3, (■) Al, Cr_2O_3.

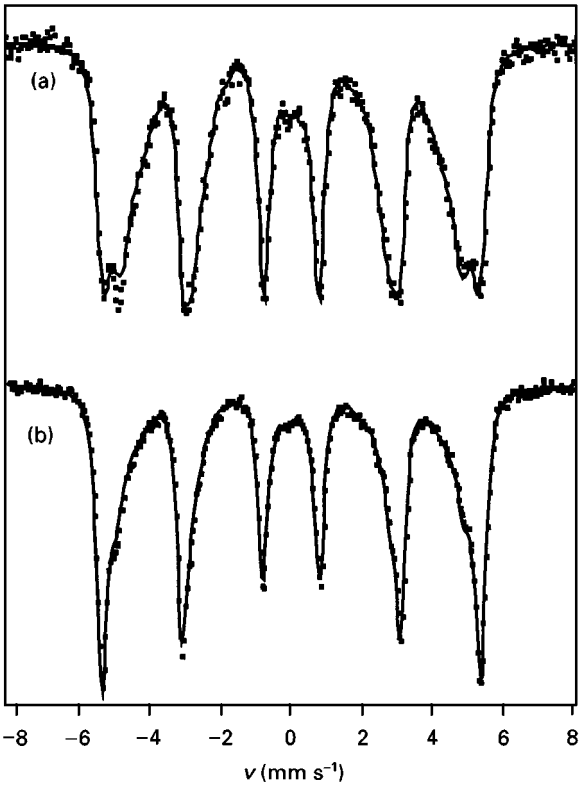

Figure 3 ^{57}Fe room-temperature Mössbauer spectra of $Fe_{0.87}Cr_{0.13}$–Al_2O_3 composites synthesized by (a) reactive milling (aluminium, iron and chromium oxide), (b) direct milling (alumina, iron and chromium). In both cases the powders were ground for 240 min.

reduction of haematite, the Mössbauer spectrum clearly shows three different iron phases (Fig. 1): the component due to haematite (Fe^{3+}) whose external lines are clearly observed on the positive and negative parts of the velocity scale, a component associated mostly with hercynite (Fe^{2+})$FeAl_2O_4$ with broad lines seen close to 0 and 2 mm s^{-1}, and a set of three clearly visible sextets associated with metallic iron–chromium (Fe^0) whose groups of external lines are close to -5 and $+5$ mm s^{-1}. After 8 h milling, the as-milled powders consist only of α-alumina and of a $Fe_{0.905}Cr_{0.095}$ alloy. The composition of the iron–chromium alloy can be calculated from the contribution of the neighbouring chromium in the first and second shells of iron atoms [33, 34] by a deconvolution of the hyperfine field distribution, further assuming a random distribution of chromium atoms in the iron matrix. We conclude that about 4–5 at % chromium are not alloyed with iron and are probably dissolved in alumina. Unfortunately, the broadening of XRD peaks, due to the small sizes of coherent diffraction domains after intensive grinding, prevent us from quantifying the amount of chromium in alumina or in the iron alloy.

Direct milling of powder mixtures of alumina, iron and chromium with the same composition as before yields a low-alloyed iron phase with only about 3 at % chromium (Fig. 3). Some unalloyed chromium must therefore remain as a separate metallic phase. Again, the presence of metallic chromium in the ground powders cannot be clearly established by XRD due to broad peaks and to the small overall amount of chromium. A longer milling time (100 h) seems to be necessary to obtain a homogeneous alloy of iron and chromium by milling in the same conditions as previously reported [28–32]. These results point out the potential of reactive milling to synthesize alumina–alloy composite powders in a reasonable time, less than 10 h, and without excessive contamination by the grinding tools.

A broad family of alumina–(iron–chromium alloy) composite powders with chromium content can thus be prepared by reactive milling. For chromium contents ranging between $x = 0.13$ and 0.50 the synthesized powders consist of α-alumina and of α-(Fe,Cr) as shown by XRD patterns. ^{57}Fe Mössbauer spectra and the associated hyperfine field distributions (HFDs) (Fig. 4), further discussed in Section 4, reveal the existence of large concentration heterogeneities in the synthesized iron–chromium alloys. For example, for $x = 0.50$, the HFD shows peaks at 330 kG and around 0 kG corresponding, respectively, to iron atoms in iron-rich and chromium-rich alloys. Such chemical heterogeneities explain why the HFD mode, that is the field at which $P(H)$ reaches its maximum, is associated with a chromium concentration larger than the average composition expected from Reaction 1.

Synthesized composite powders may be made homogeneous by thermal treatments. As shown by Mössbauer HFDs (Fig. 5) of alumina–(Fe,Cr) powders, heated at 1100 °C for 1 h, the previous peaks around 0 and 330 kG are no longer observed, while the HFD maxima are shifted to larger fields and the standard deviations decrease (Table I). The compositions calculated from the average hyperfine field are lower than the initial compositions. Such differences may come from chromium dissolved in alumina and (/or) from supermagnetic Fe–Cr clusters as discussed below (Section 4.1).

3.2. Alumina–(Fe,Ni) systems

Reactive milling mechanisms which lead to the synthesis of alumina–(Fe,Ni) composites were studied

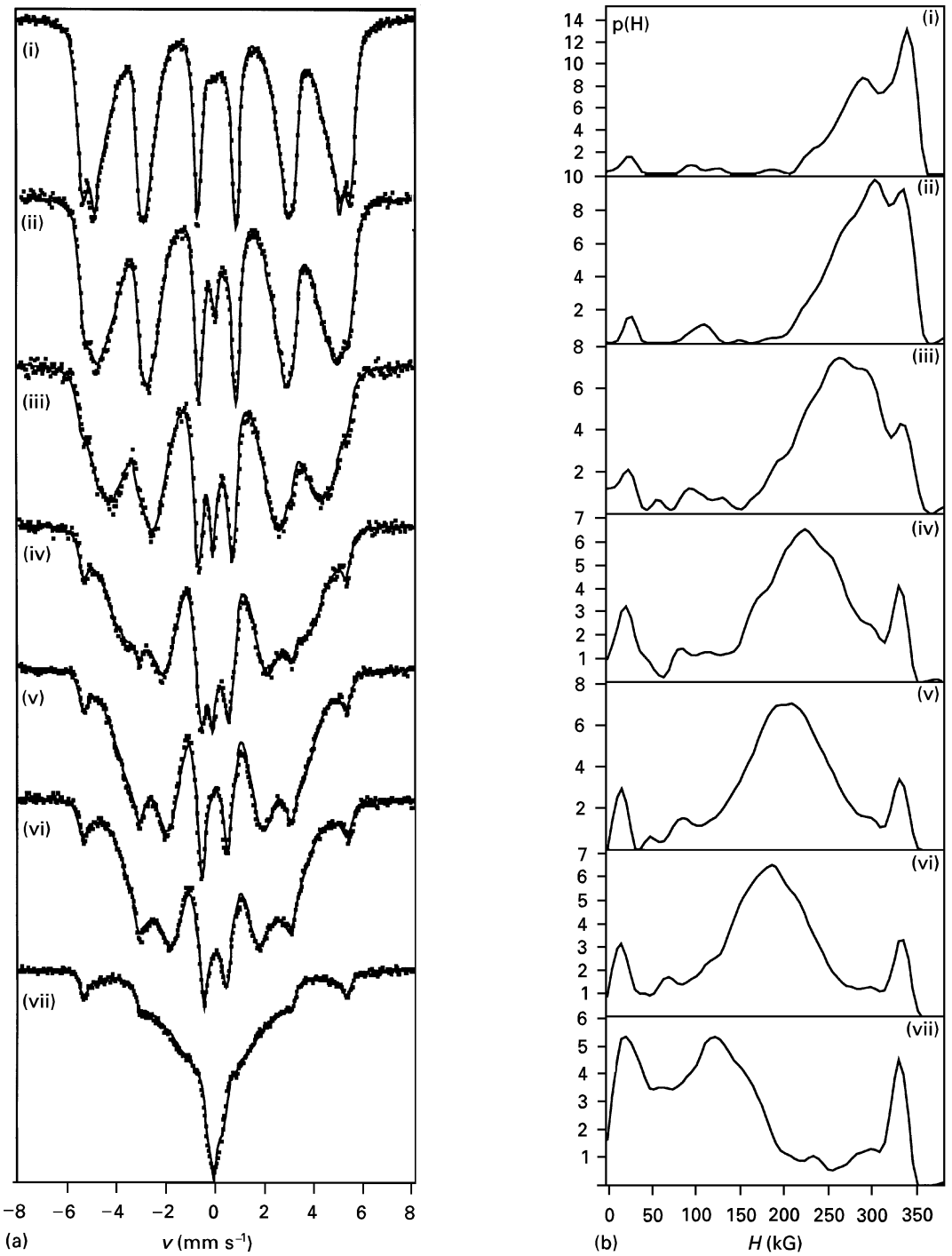

Figure 4 (a) ^{57} Fe Mössbauer spectra at room temperature and (b) associated hyperfine field distributions of $Fe_{1-x}Cr_x$–Al_2O_3 powders synthesized by reactive milling (480 min). x = (i) 0.13, (ii) 0.20, (iii) 0.30, (iv) 0.40, (v) 0.45, (vi) 0.50, (vii) 0.60.

with the Al_2O_3–$Fe_{0.70}Ni_{0.30}$ composition. An incubation milling time of 25–30 min before the start of the reaction is observed. The corresponding XRD patterns (Fig. 6) show the presence of α-Al_2O_3 and α-(Fe,Ni) alloys after long milling times (Fig. 6b). The reaction mechanism, however, is not straightforward, as evinced by a number of transient phases which can be detected (Fig. 6a) after short milling periods, namely γ-(Fe,Ni) and hercynite $FeAl_2O_4$ besides unreacted Fe_2O_3. Also to be noted are diffraction peaks which may be attributed to some Ni–Al–O phase(s) which were first reported by Colin [35]. Such metastable Al_2O_3-rich nickel aluminates appear during cooling the superstoichiometric stable spinel phase as part of the Al_2O_3 exsolution mechanism [35] in a manner similar to what has also been found to occur in the MgO–Al_2O_3 system [36]. They eventually disappear from conventionally prepared samples upon reheating to $\geqslant$1000 °C. The associated Mössbauer spectra (Fig. 7) are composed of four subspectra (Table II) characteristic of haematite, hercynite and the α-(Fe,Ni) and γ-(Fe,Ni) alloys. The γ-(Fe,Ni) alloy, which is non-magnetic at room temperature, corresponds thus to a composition in the range from 25–30 at % Ni.

In all Al_2O_3–$Fe_{(1-y)}Ni_y$ composites studied here, the phases synthesized after 8 h milling are α-alumina and α and γ-Fe–Ni alloys whatever the starting

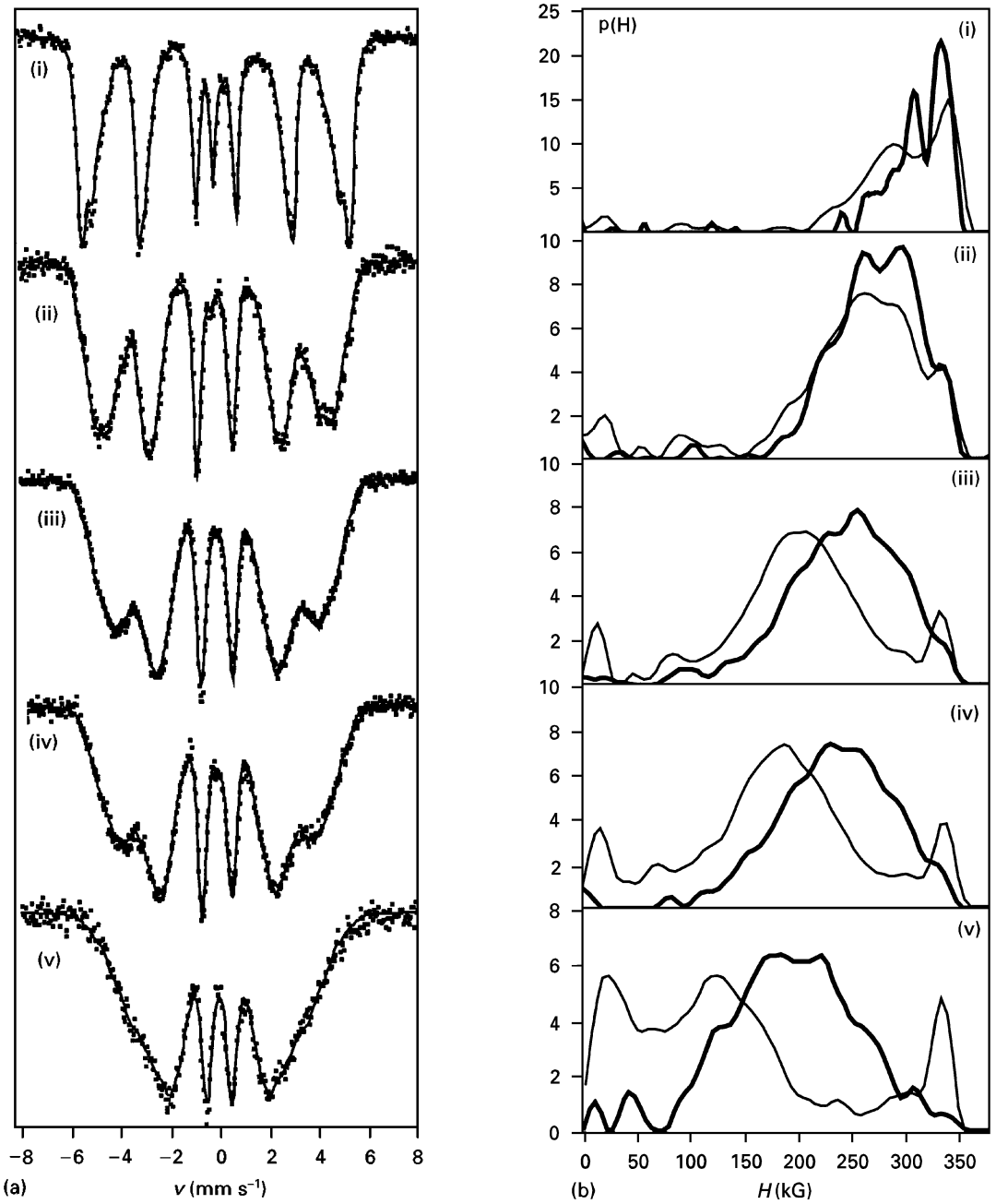

Figure 5 (a) ^{57}Fe room-temperature Mössbauer spectra and (b) corresponding hyperfine field distributions (HFD, ——) of $Fe_{1-x}Cr_x$–Al_2O_3 powders produced by reactive milling (480 min) and subsequently heat treated at 1100 °C for 1 h. x = (i) 0.10, (ii) 0.30, (iii) 0.45, (iv) 0.50, (v) 0.60. HFDs of the same samples before heat treatment.

composition y (Fig. 8). The fractions of both iron–nickel alloys were calculated by deconvoluting the corresponding HFDs (Fig. 9). The components of the HFDs with a field larger than $H_b \approx 320$ kG are attributed to b c c α-Fe–Ni alloys, while those with a field smaller than H_b correspond to f c c γ-Fe–Ni alloys [37, 38]. Fig. 10 shows that the relative areas of the b c c component are still ≈ 0.10 even for y values as large as 0.60 or 0.80. The coexistence of b c c and f c c phases has been reported recently by Hong and Fultz [39] in ball-milled Fe–Ni alloys and by Huang *et al.* [40] in a ground 304 stainless steel. The range of coexistence of the two Fe–Ni phases [39] depends on the milling intensity, the nickel content ranging typically between 0.12 and 0.30. In that range, both phases have the same composition. Such results have been explained by a higher defect density in the b c c alloys than in the f c c alloys with heterogeneous defect densities throughout the alloys. In the case of ground 304 stainless steel, Huang *et al.* [40] explained their results by a strain-induced martensitic transformation which occurs during milling. As before, composite powders can be homogenized by annealing, and a change of the fraction of the synthesized α and γ alloys also takes place (Fig. 11 and Section 4.2).

3.3. Alumina–(Fe,Cr,Ni) systems

In all the alumina–(Fe,Cr,Ni) systems studied in the present work, the final phases, after 8 h milling, consist of α-alumina, γ- and α-iron alloys whatever the initial compositions (Fig. 12). Considering that the α and the

TABLE I Mean hyperfine field, $\langle H \rangle$ and standard deviation, σ, of $P(H)$ for two typical Al_2O_3–$Fe_{1-x}Cr_x$ powders synthesized by reactive milling (8 h) before and after heat treatment to 1100 °C for 1 h. The chromium content (atomic fraction of chromium), x, is calculated from $\langle H \rangle$ using the results of Dubiel and co-workers [33, 34]

Expected chromium content		$\langle H \rangle$ (kG)	σ (kG)	True chromium content
0.30	As-milled	242	80	0.29
	Heat-treated	270	50	0.20
0.50	As-milled	180	84	0.49
	Heat-treated	232	57	0.33

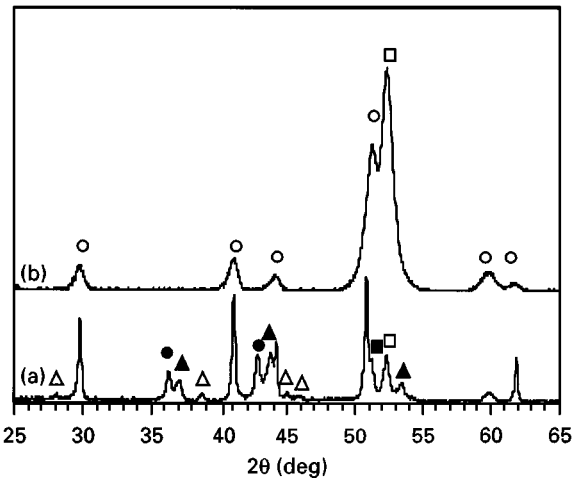

Figure 6 X-ray diffraction patterns of Al_2O_3–$Fe_{0.70}Ni_{0.30}$ powders for different milling times: (a) 30 min, (b) 480 min. (●) $FeAl_2O_4$, (□) α-Fe,Ni, (■) γ-Fe,Ni, (○) α-Al_2O_3, (▲) Ni–Al–O, (△) Fe_2O_3.

γ phases are, respectively, characterized in Mössbauer spectrometry at room temperature by a magnetic and a non-magnetic subspectrum (Fig. 12), their relative area fractions have been determined (Table III). Even with a high nickel content it was impossible to synthesize the γ-alloys only. Such results agree with those of Fe–Ni composites and with those of Huang *et al.* [40] for 304 stainless steel ($Fe_{0.738}Cr_{0.186}Ni_{0.076}$) discussed in the previous section.

Some as-milled powders have been subsequently annealed (1100 °C, 1 h). In that way, γ-alloy–alumina composite powders can be synthesized. For the $Fe_{0.60}Cr_{0.18}Ni_{0.22}$–$Al_2O_3$ composite, the phases identified from XRD patterns are indeed only α-alumina and a γ-iron alloy. This is confirmed by the Mössbauer spectrum of Fig. 13 where no magnetic component is observed.

4. Discussion

4.1. Alumina–(Fe,Cr) systems

A hyperfine field of atoms at interfaces (boundaries between metallic grains, interfaces between metallic grains and alumina) may explain part, but not all, of the low-tail field of the HFDs: the fraction of iron atoms at interfaces cannot be larger than ≈20% for the typical coherent domain size measured here (15–20 nm). Their fields, H_{int}, are reduced by about 5%–10% in iron-rich alloys [41] and possibly more in chromium-rich alloys as compared to fields of atoms in grains. The concentration dependence of the mean hyperfine field $\langle H \rangle_{h\ sol\ sol}$ of a homogeneous $Fe_{1-x}Cr_x$ alloy is well accounted for by a linear variation for $0.02 \leqslant x \leqslant 0.50$ with a slope of about -310 kG from various literature results. For a mixture of solid solutions with coarse grains, the average chromium content may thus be estimated from the average field $\langle H \rangle_{sol\ sol}$. Table I gives the chromium contents which are calculated from the average hyperfine field $\langle H \rangle (x_{calc} = (334.3 - \langle H \rangle)/313.8)$, a relation deduced for $x \geqslant 0.02$ from the averages fields $\langle H \rangle_A$ published

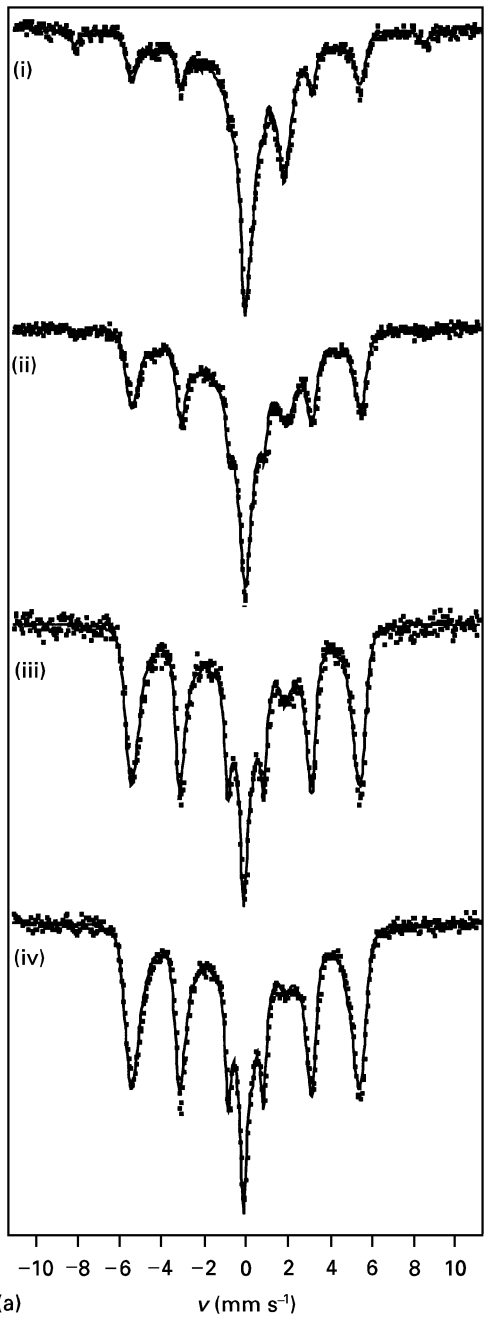

Figure 7 (a) ^{57}Fe room-temperature Mössbauer spectra of Al_2O_3–$Fe_{0.70}Ni_{0.30}$ powders and (b) corresponding hyperfine field distributions as a function of milling time: (i) 30 min, (ii) 60 min, (iii) 120 min, (iv) 240 min.

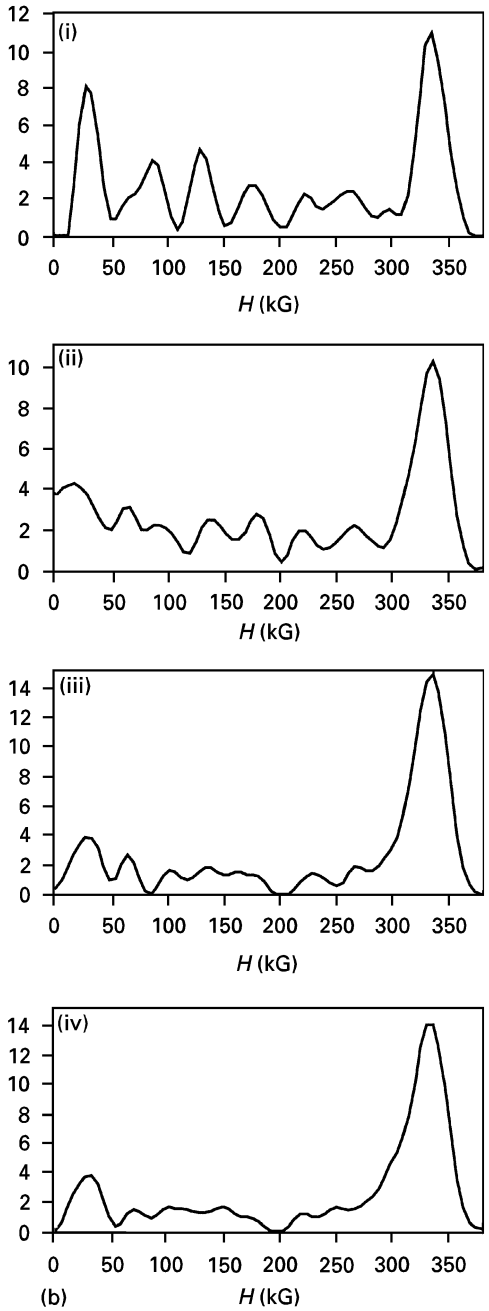

Figure 7 (*continued*)

by Dubiel and co-workers [33, 34] by assuming that it represents the latter average field $\langle H \rangle_{\text{sol sol}}$, i.e., by neglecting the contributions of interfaces. As $\langle H \rangle$ is smaller than the actual field of the sole Fe–Cr solid solutions, the calculated chromium contents are overestimated, despite the agreement between the estimated values and the y Cr contents of the initial powder mixtures shown in Table I. This explains why different concentrations are, for instance, calculated for $y = 0.13$ from $\langle H \rangle$ (0.13) and from a direct deconvolution of some peaks of the HFD, as explained above (0.095). The previous discussion also implies that part of the chromium is either uncombined or is dissolved in alumina [42].

After heat treatment, the Mössbauer spectrum of as-milled Al_2O_3–$Fe_{0.87}Cr_{0.13}$ consists of two main subspectra: a sextuplet corresponding to an 8 at % Cr

TABLE II Mössbauer hyperfine parameters of $Fe_{0.70}Ni_{0.30}$–Al_2O_3 composite powders milled for 30 min

	Relative area	H (kG)	IS (mm s^{-1})	EQ (mm s^{-1})
Fe^{3+}	0.05	515	0.18	0.01
Fe^{2+}	0.41	0	0.95	1.7
α-Fe	0.35	336	0.01	0
γ-Fe	0.19	0	0.08	0

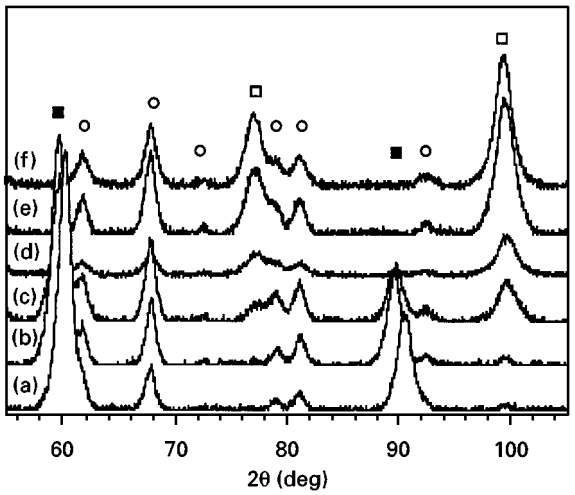

Figure 8 X-ray diffraction patterns of Al_2O_3–$Fe_{(1-y)}Ni_y$ powders prepared by reactive milling (480 min). (a) $y = 0.80$, (b) $y = 0.50$, (c) $y = 0.35$, (d) $y = 0.25$, (e) $y = 0.20$, (f) $y = 0.10$. (□) α-Fe,Ni, (■) γ-Fe,Ni, (○) α-Al_2O_3.

Fe–Cr alloy and a singlet with an isomer shift of -0.11 ± 0.02 mm s^{-1}. The latter singlet is also close but significantly shifted with respect to the singlet line attributed to superparamagnetic iron clusters in alumina [43, 44] (IS close to 0, typically -0.02, -0.03 mm s^{-1}). The singlet line cannot be associated with sigma phase whose isomer shift is -0.19 ± 0.02 mm s^{-1} [45]. Using the relative areas of the two subspectra (0.92 and 0.08 for the magnetic and non-magnetic components, respectively) and an initial chromium content of 0.095 in an Fe–Cr alloy, it is possible to estimate the chromium concentration of the chromium-rich phase as being of the order of 0.3. Classical Fe–Cr alloys with such chromium contents are magnetic at room temperature. Although the singlet isomer shift is consistent with a chromium-rich Fe–Cr alloy non-magnetic at RT (for instance, IS $= -0.12$ mm s^{-1} for ≈ 70 at % Cr), the latter concentration evaluation suggests that the singlet is more likely associated with superparamagnetic Fe–Cr clusters in alumina. In conclusion, reactive milling followed by annealing allow synthesis of alumina–(Fe–Cr) composites in a wide alloy composite range, and with presumably unusual nanoscale microstructures.

4.2. Alumina–(Fe,Ni) systems

It must be pointed out that the HFD shows a broad band between $H = 0$ and $H_b \approx 320$ kG whose main part can only be attributed to a set of γ alloys with

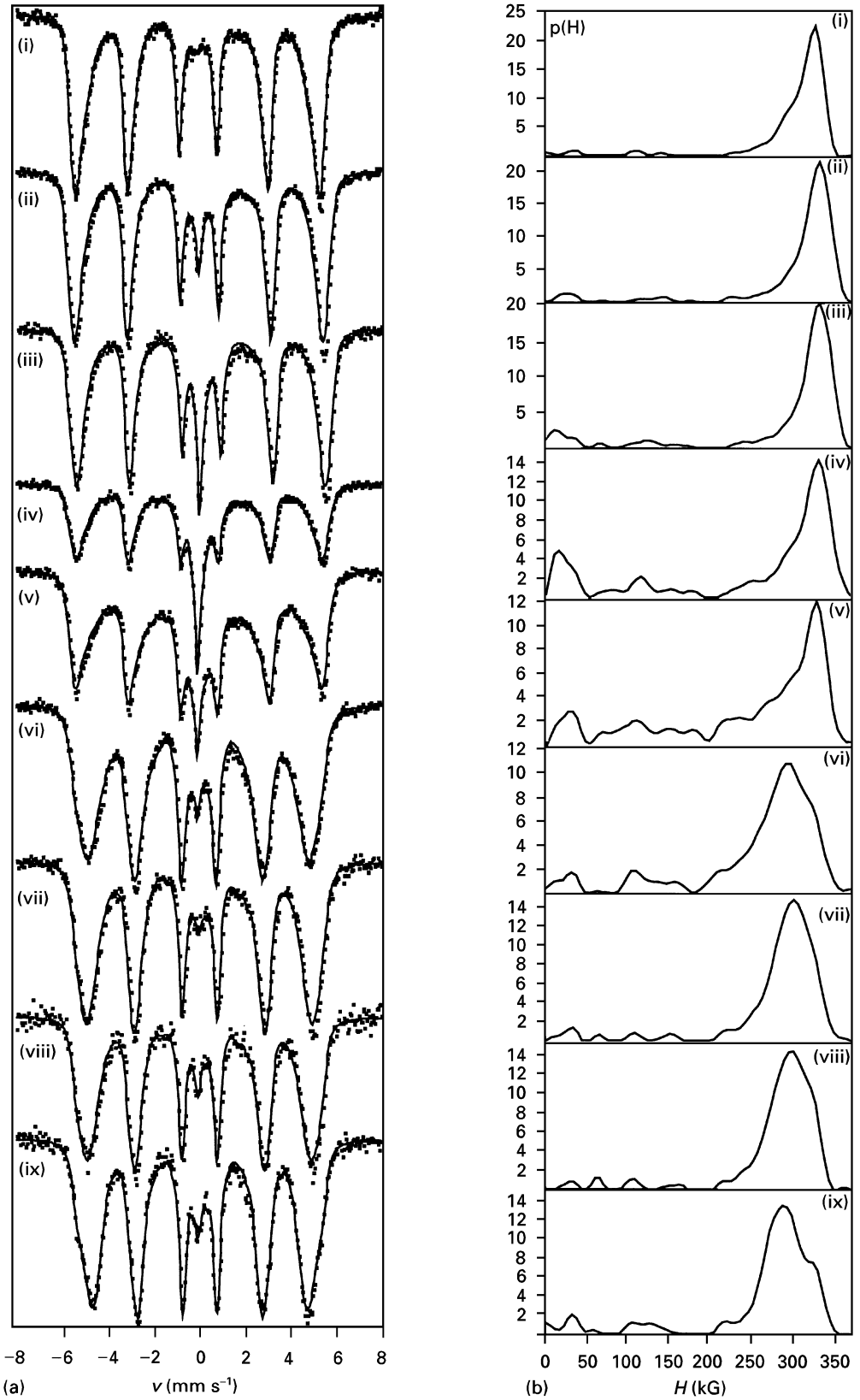

Figure 9 (a) ^{57}Fe room-temperature Mössbauer spectra and (b) corresponding hyperfine field distributions of Al_2O_3–$Fe_{(1-y)}Ni_y$ powders synthesized by reactive milling (480 min). y = (i) 0.10, (ii) 0.20, (iii) 0.25, (iv) 0.30, (v) 0.35, (vi) 0.40, (vii) 0.50, (viii) 0.60, (ix) 0.80.

various compositions [37, 38], a smaller part being due to iron atoms at interfaces and grain boundaries as discussed in the previous section for Fe–Cr alloys. The alloys become progressively homogeneous as milling proceeds while haematite is totally reduced and hercynite is no longer observed after milling for 100 and 480 min, respectively. The observation of both iron–aluminium and nickel–aluminium oxides during the progression of the reaction is in accordance with previous works which showed the formation of spinel oxides as transient phases [14, 46].

The strong variation of the average hyperfine field of the γ-alloys with composition allows estimation of an average nickel content of f c c alloys (Table IV). By

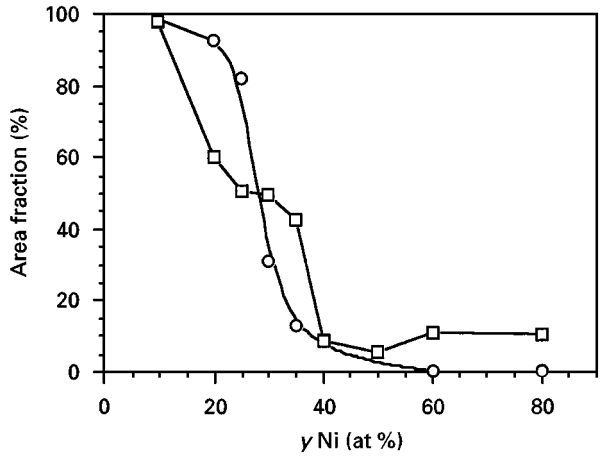

Figure 10 Area fraction, A (%) of the α-(Fe,Ni) phase in $Fe_{1-y}Ni_y$–Al_2O_3 powders synthesized (a) by reactive milling (480 min, —□—), (b) by reactive milling (480 min, —□—) followed by annealing at 1100 °C for 1 h. The area fraction of γ-(Fe,Ni) alloy is 100-A.

contrast, the weak variation of the average hyperfine field of α-alloys with composition, cannot be used to estimate the nickel content of the α-alloys. The lattice parameter of the α-(Fe,Ni) phase, calculated from the XRD patterns, tends to reach the value of pure b c c iron ($a_{Fe} = 0.286\,64$ nm) for the largest contents y of nickel in the starting powders. However, the latter result does not prove that the nickel content of the corresponding b c c alloys is small, as the lattice parameter of b c c alloys varies only slightly with nickel content and is close to the pure iron value for a content larger than 0.25. Moreover, the lattice parameters reported by Hong and Fultz [39] decrease slightly below the pure iron value for a nickel content larger than about 0.20. Our results are thus also consistent with a coexistence of b c c and f c c iron-rich nickel alloys in the concentration range discussed by Hong and Fultz [39], a coexistence which is here a consequence of the heterogeneities observed in the powders at the beginning of the reaction.

For the alumina–(Fe,Cr) systems, composite powders can be homogenized by annealing, and a change in the fraction of the synthesized α and γ alloys also takes place (Fig. 11). The chemical homogenization is revealed by the diminution of the standard deviation, σ, of the HFD. For example, for $y = 0.20$, σ is, respectively, 67 and 44 kG before and after heating. Although their amounts have strongly decreased, it is worth noticing that a clear contribution of b c c Fe–Ni alloy is still observed in Mössbauer spectra of annealed samples which have a nickel content y comprised between 0.25 and 0.35. As the f c c phase is the only expected equilibrium phase, equilibrium has thus not been reached. The latter domain of phase coexistence is in agreement with the previous discussion about as-milled Fe–Ni alloys.

5. Conclusion

Mössbauer spectroscopy and X-ray diffraction were used to investigate the synthesis by reactive milling of nanocomposite powders which consist mainly of alumina and of alloys either binary or ternary in the (Fe,Cr,Ni) system. More particularly (Fe,Cr) and (Fe,Ni) alloys with chromium contents ranging between 0.13 and 0.60 and nickel contents between 0.10 and 0.80 respectively, have been considered. Some compositions have also been investigated in the iron-rich part of the ternary system. In all cases, chemical and structural heterogeneities of the metallic components of the ground nanocomposites have been demonstrated and characterized semi-quantitatively from

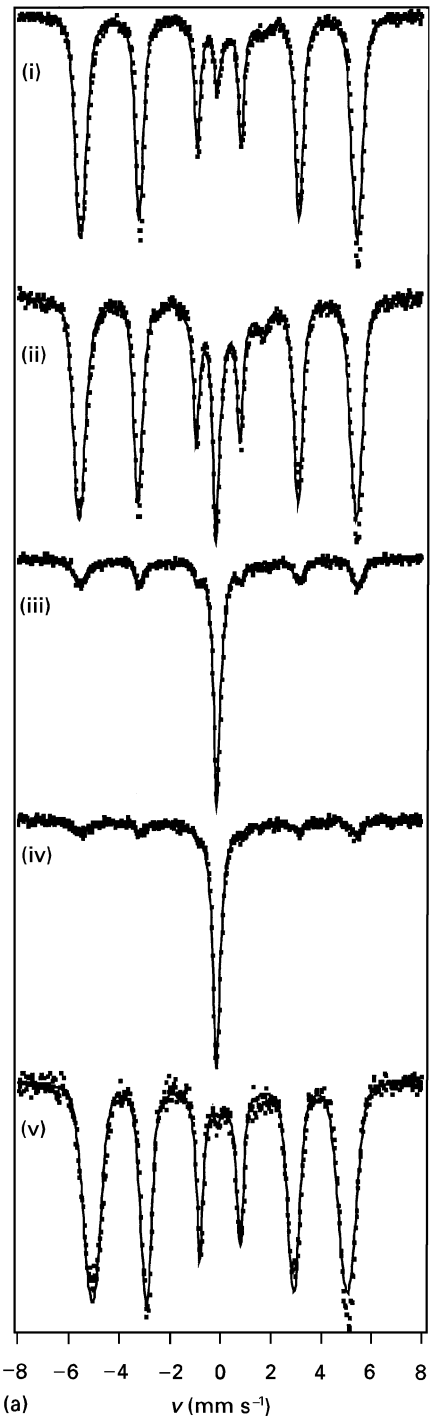

Figure 11 (a) ^{57}Fe room-temperature Mössbauer spectra and (b) corresponding hyperfine field distributions (HFD, ——) of $Fe_{1-y}Ni_y$–Al_2O_3 composite powders prepared by reactive milling (480 min) and subsequently heat treated at 1100 °C for 1 h. y = (i) 0.20, (ii) 0.25, (iii) 0.30, (iv) 0.35, (v) 0.60. (——) HFDs of the same samples before heat treatment.

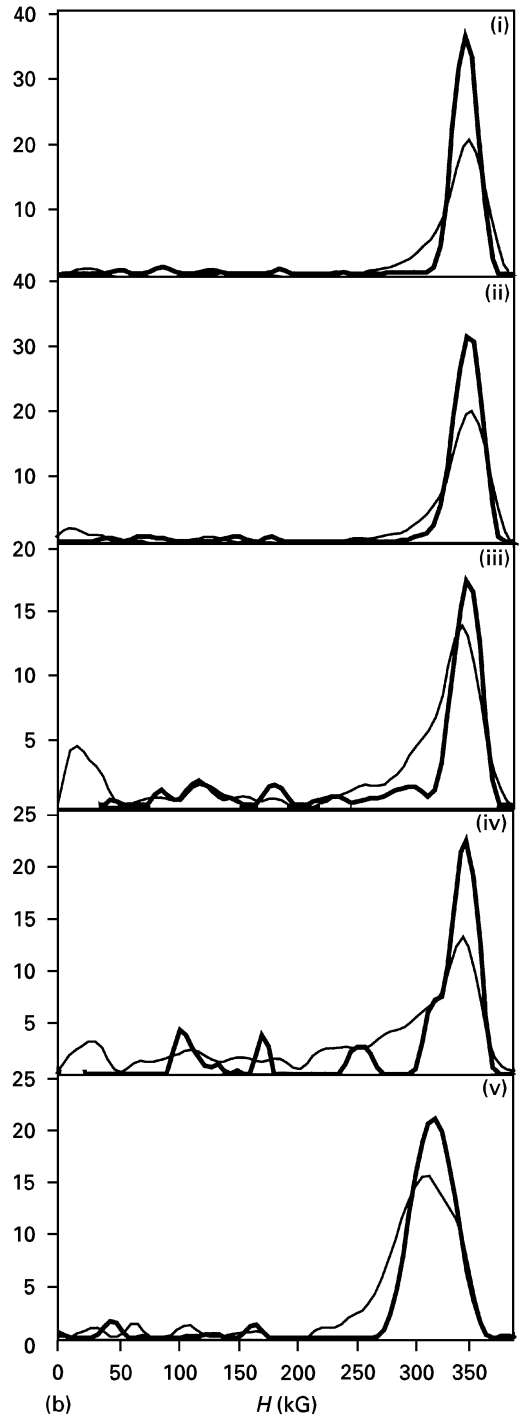

Figure 11 (*continued*)

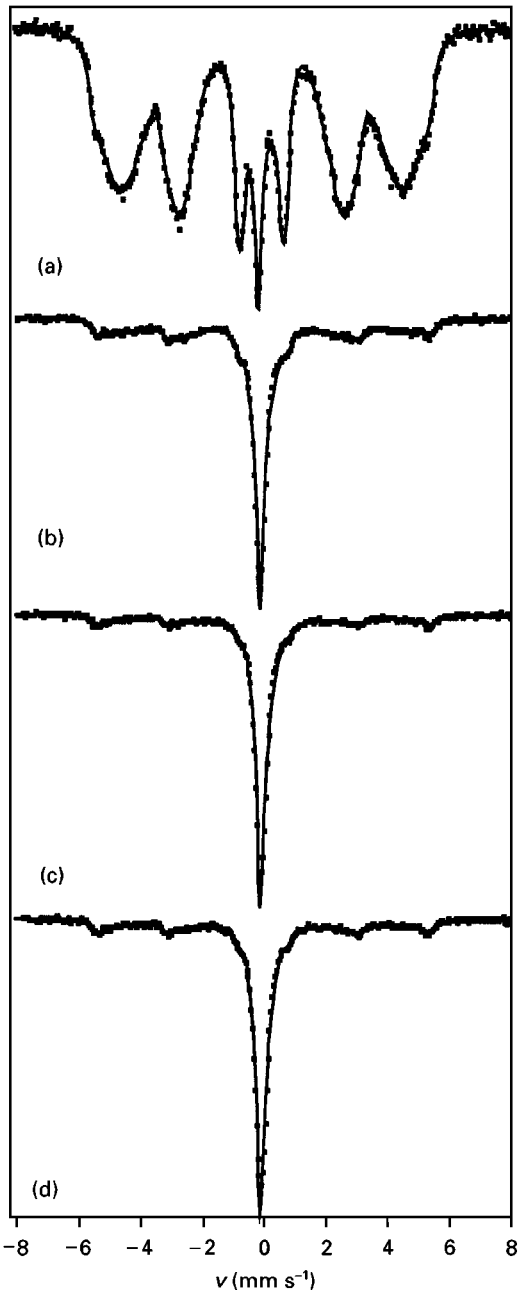

Figure 12 ^{57}Fe room-temperature Mössbauer spectra of Al_2O_3–$Fe_{(1-x-y)}Cr_xNi_y$ powders synthesized by reactive milling (480 min). $1-x-y/x/y$: (a) 0.72/0.20/0.08, (b) 0.64/0.20/0.16, (c) 0.58/0.20/0.22, (d) 0.60/0.18/0.22.

room-temperature Mössbauer spectra. The possibility of side effects such as partial dissolution of not yet reacted Cr_2O_3 into newly formed Al_2O_3 has also been considered. Subsequent heat treatments of the as-milled powders may be performed at reasonably low temperatures to convert the latter into structurally and chemically homogeneous composite powders. The possibility of monitoring the final alloy composition has thus been evinced in a ternary system with important potentialities. Profit may be taken from the necessary consolidation step during subsequent powder processing to reach the latter homogeneous state.

TABLE III Area fractions of the Mössbauer subspectra associated with the γ alloys as a function of the initial composition of the Al_2O_3–$Fe_{(1-x-y)}Cr_xNi_y$ powder mixtures

Composition Cr/Ni, balance Fe	Area fractions	
	Milling (8 h)	Milling and annealing (1100 °C, 1 h)
0.20/0.08	0.14	0.52
0.20/0.16	0.65	
0.18/0.22	0.71	1.00
0.20/0.22	0.78	

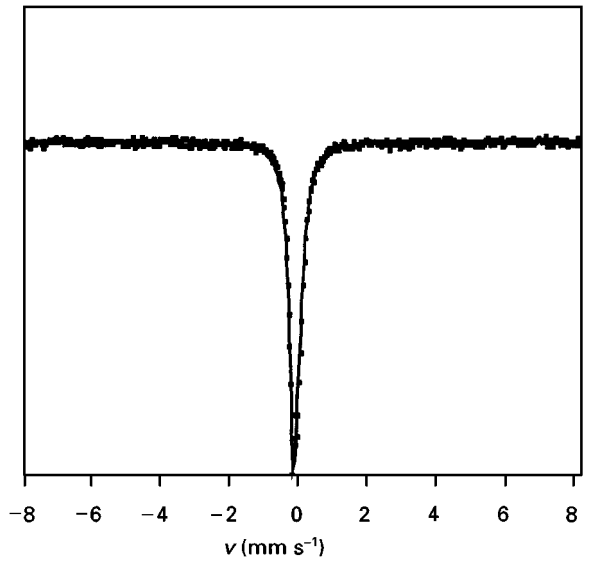

Figure 13 ^{57}Fe room-temperature Mössbauer spectra of Al_2O_3–$Fe_{0.60}Cr_{0.18}Ni_{0.22}$ powders synthesized by reactive milling (480 min) and annealed at 1100 °C for 1 h.

TABLE IV Comparison of expected and calculated nickel contents in Al_2O_3–$Fe_{(1-y)}Ni_y$ composite powders

Expected nickel content in Al_2O_3–$Fe_{(1-y)}Ni_y$	Mode of the hyperfine field distribution (kG)	Calculated nickel content
0.80	294	0.70
0.60	308	0.58
0.50	313	0.50
0.40	300	0.38

Acknowledgement

P. Delcroix is gratefully acknowledged for his skillful help in Mössbauer spectroscopy.

References

1. T. S. SHELVIN, in "Cermets", edited by J. R. Tinklepaugh and W. R. Crandall (Reinhold, New York, 1960) p. 97.
2. W. H. TUAN and R. J. BROOK, *J. Europ. Ceram. Soc.* **6** (1990) 31.
3. Y. NAERHEIM, *Powder Metall. Int.* **18** (1986) 158.
4. A. G. EVANS, M. C. LIU, S. SCHMAUDER and M. RÜHLE, *Acta Metall.* **34** (1986) 1643.
5. M. NAWA, T. SEKINO and K. NIIHARA, *J. Mater. Sci.* **29** (1994) 3185.
6. E. BREVAL, Z. DENG, S. CHIOU and C. G. PANTANO, *ibid.* **27** (1992) 1464.
7. W. H. TUAN and R. J. BROOK, *Br. Ceram. Soc. Proc.* **46** (1990) 335.
8. D. OSSO, A. MOCELLIN, G. LE CAËR and A. PIANELLI, *J. Phys. IV* **3** (1993) 1311.
9. C. H. HENAGER and J. L. BRIMHALL, *Scripta Metall.* **29** (1993) 1597.
10. A. MARCHAND, X. DEVAUX, B. BARBARA, P. MOLLARD, M. BRIEU and A. ROUSSET, *J. Mater. Sci.* **28** (1993) 2217.
11. K. NIIHARA, A. NAKAHIRA and T. SEKINO, *Mater. Res. Soc. Symp. Proc.* **286** (1993) 405.
12. K. NIIHARA, *Seramik. Kyokai Gakujutsu Ronbunshi* **99** (1991) 974.
13. L. L. WANG, Z. A. MUNIR and Y. M. MAXIMOV, *J. Mater. Sci.* **28** (1993) 3693.
14. P. MATTEAZZI and G. LE CAËR, *J. Am. Ceram. Soc.* **75** (1992) 2749.
15. L. TAKACS, *Nanostruct. Mater.* **2** (1993) 241.
16. M. PARDAVI-HORVATH and L. TAKACS, *J. Appl. Phys.* **73** (1993) 6958.
17. G. B. SCHAFFER and P. G. McCORMICK, *Appl. Phys. Lett.* **55** (1989) 45.
18. T. D. SHEN, K. Y. WANG, M. X. QUAN and J. T. WANG, *Scripta Metall.* **25** (1991) 2143.
19. G. B. SCHAFFER and P. G. McCORMICK, *Metall. Trans.* **21A** (1990) 2789.
20. *Idem*, *J. Mater. Sci. Lett.* **9** (1990) 1014.
21. *Idem*, *Metall. Trans.* **22A** (1991) 3019.
22. H. YANG and P. G. McCORMICK, *J. Solid State Chem.* **110** (1994) 136.
23. L. TAKACS, *Mater. Lett.* **13** (1992) 119.
24. G. B. SCHAFFER and P. G. McCORMICK, *Scripta Metall.* **23** (1989) 835.
25. P. MATTEAZZI, M. D. BASSET, D. OSSO, G. LE CAER, S. BEGIN-COLIN and A. MOCELLIN, in "Powder Metallurgy World Congress", Les Editions de Physique, Vol. III (Paris, 1994) p. 1815.
26. C. KUHRT and L. S. SCHULTZ, *J. Appl. Phys.* **73** (1993) 1975.
27. L. R. DE ARAUJO PONTES, Thesis INPL, Nancy, France (1993).
28. H. KUWANO, H. OUYANG and B. FULTZ, *Nanostruct. Mater.* **1** (1992) 143.
29. J. HESSE and A. RUBARTSCH, *J. Phys. E Sci. Instrum.* **7** (1974) 526.
30. G. LE CAËR and J. M. DUBOIS, *ibid.* **12** (1979) 1083.
31. D. OSSO, Thesis INPL, Nancy, France (1995).
32. T. KOYANO, T. TAKISAWA, T. FUKUNAGA and U. MIZUTANI, *J. Appl. Phys.* **73** (1993) 429.
33. S. M. DUBIEL and K. KROP, *J. Phys. Coll. C6* **12** (1974) 459.
34. S. M. DUBIEL and J. ZUKROWSKI, *J. Magn. Magn. Mater.* **23** (1981) 214.
35. F. COLIN, *Rev. Int. Hautes Temp. Refract.* **5** (1968) 267.
36. A. M. LEJUS, *Rev. Int. Hautes Temp. Refract.* **1** (1964) 53.
37. D. G. RANCOURT and J. Y. PING, *Hyp. Int.* **69** (1991) 497.
38. M. FOSS, C. FRANTZ and G. LE CAËR, *Scripta Metall.* **21** (1987) 325.
39. L. B. HONG and B. FULTZ, *J. Appl. Phys.* **79** (1996) 3946.
40. H. HUANG, J. DING and P. G. McCORMICK, *Mater. Sci. Eng. A* **216** (1996) 178.
41. L. DAROCZI, D. L. BECKE G. POSGAY and M. KIS-VARGA, *Nanostruct. Mater.* **6** (1995) 981.
42. M. RISTIC, S. POPOVIC and S. MUSIC, *Mater. Lett.* **16** (1993) 309.
43. C. J. McHARGUE, P. S. SKLAD, C. W. WHITE, G. C. FARLOW, A. PEREZ and G. MAREST, *J. Mater. Res.* **6** (1991) 2145.
44. P. MATTEAZZI, F. MIANI and D. BASSET, *Nanostruct. Mater.* **2** (1993) 355.
45. B. F. O. COSTA and S. M. DUBIEL, *Phys. Status Solidi* (*a*) **139** (1993) 83.
46. D. OSSO, O. TILLEMENT, G. LE CAËR and A. MOCELLIN, in Proceedings of the 8th CIMTEC World Ceramic Congress, Florence, June 29–July 4, 1994 (C.R.C.) in press.

Received 7 February 1997
and accepted 3 March 1998